Shallow Lithosphere-Asthenosphere Boundary beneath Cambay Rift Zone of India: Inferred Presence of Carbonated Partial Melt

Prakash Kumar[1], Gautam Sen[2], Prantik Mandal[1] and Mrinal K. Sen[3]

[1]CSIR - National Geophysical Research Institute, Hyderabad, India
[2]Dean, School of Natural & Social Sciences, Lehman College (CUNY), New York, USA
[3]Institute for Geophysics, The University of Texas at Austin, USA
Email: [1]prakashk@ngri.res.in; [2]sengorama@gmail.com; [1]prantik@ngri.res.in; [3]msentx@gmail.com

Abstract: Cambay Rift Zone (CRZ) is an ancient rift that had last witnessed volcanism and rifting activity 68-65 million years ago, when the Indian plate migrated over the Deccan plume, potentially signifying the presence of a shallow LAB. Here we apply converted wave techniques to a teleseismic earthquake dataset to image the mantle below the CRZ. We place the Lithosphere-Asthenosphere Boundary (LAB) beneath this rift at a depth where a ~10% drop occurs in shear wave velocity. The seismic velocity structure indicates that the lithosphere thickness varies from ~60 km beneath the rift to ~110 km beneath rift walls. Furthermore, the upper mantle discontinuities (410 and 660 km discontinuities) are found to be thinner by ~2 sec (i.e. ~20km) with delayed 410-km discontinuity and normal 660-km discontinuities. We infer this to be caused by a thermal anomaly in the upper mantle. The surface heat flow at CRZ is high. A geothermal gradient extrapolated from the surface heat flow intercepts CO_2-bearing mantle peridotite solidus at 60 km, and thus could signal the presence of small amounts of carbonatite-type magma. We suggest that the CRZ might become reactivated by the generation of small pockets of melt at the LAB, which is being triggered by a thermal anomaly in the upper mantle beneath this currently inactive rift.

Keywords: Asthenosphere, Cambay rift zone, Deccan

INTRODUCTION

Continental rift zones form in passive response to plate extensional forces or due to the presence of a thermal anomaly in the upper mantle. Continued extension may lead to complete separation of the two sides of the rifted zone and formation of an ocean basin; and in other cases a rift may stop extending further after the initial separation, i.e., it may become an inactive (failed) rift. The Indian continent has several major rift zones that formed during the separation of Gondawanaland (Biswas, 1987). Here we focus on the present day activities beneath the Cambay rift zone (CRZ; Fig. 1) in northwest India, which is well known for its oil and gas reserves.

The CRZ is defined by a series of longitudinal faults and several cross faults (inset in Fig. 1). The rift basin is believed to have formed by extension that occurred between 65 Ma, when the Deccan erupted, during the Eocene/ Paleocene time (Biswas, 1987). Although the CRZ is presumed to fall on the path of the Deccan-Reunion plume/ hot spot track (Mahoney et al., 2002), it is unclear how the extension was related to such plume activity. This is because there is no evidence of an initial doming of the area, as is

the case of the Baikal rift zone, where a tomographic study suggested doming of the lithosphere due to plume activity (Zhao et al., 2006).

Seismic studies and examination of drill cores through the CRZ have revealed a stratigraphy that shows a basement of Deccan Trap basalts (Fig. 2). Above this basement occur sedimentary beds of the Olpad Formation that are composed of conglomerate (with pebbles of Deccan lava), wacke, and sandstone. They appear to have been deposited as alluvial fans, fan deltas in lacustrine environments (Mohan, 1995). Marine incursion is evident from the overlying thick sequence of Cambay shale, which are largely comprised of dark colored shales. The overlying sediments, representing the younger Tertiary and Quaternary, are terrestrial in origin, indicating retreat of the sea following the deposition of Cambay Shale (Mohan, 1995).

This region is ideal to test the interaction of plumes-lithosphere-rift system. The seismic propagation is primarily affected by the temperature and the medium (composition). Therefore, our aim is to test whether the nature of upper mantle seismic discontinuities are thermally and/or compositionally dominated. Here we used a converted wave
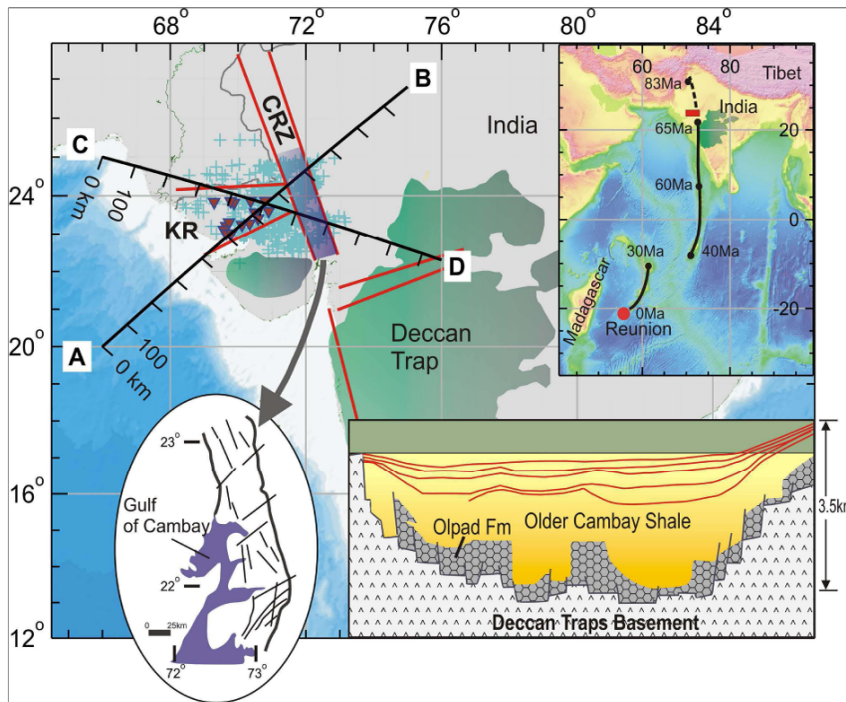
Fig.1. Map with broadband seismic station distribution and profiles. AB and CD are two profiles with tick marks along which the seismic sections have been analyzed in Fig. 2. Red inverted tingles are the broadband seismic stations. Crosses (in cyan) around the stations are the conversion points at a depth of 100 km for S-to-p waves. The major rifts (taken from Biswas, 1987) are also shown in red. CRZ: Cambay Rift zone, NR: Narmada rift and KR: Kachchh Rift. The extent of Deccan basalt in western and central India is also shown. The key map in the right top shows the present day location of Reunion and the approximate track of the hotspot (thick black line). The dash black line in north is the further extent of the hotspot track (Mahoney et al., 2000; Basu et al., 1993). The numbers in the key map indicates the position of hotspot in Ma. The small rectangle in red color in key map is our study region. The inset in lower left (in oval) indicates the zoomed version of a portion of Cambay Rift Zone (shaded region) and a geological section is also shown in the lower right. The geological section shows the marine inclusion of the thick shale of early Eocene.

technique, which utilizes shear-to-compressional conversion to image the upper-most mantle structure of the entire region. We show that our results are consistent with a model of a thinned lithosphere that is underlain by a LAB with small amounts of carbonatite magma; and also infer that a thermal plume rising through the upper mantle is responsible for the increased temperature at the LAB.

DATA AND METHOD

Here we present a seismic image of the upper mantle beneath Cambay rift obtained by using a converted wave technique, namely, compressional-to-shear waves (PRF) and shear-to-compressional waves (SRF) wave (also called converted waves) receiver functions from teleseismic data (Vinnik, 1977; Langston, 1995; Fara and Vinnik, 2000). The

PRF and SRF are generated from vertical and horizontal components of ground motion recorded at the seismic station. A PRF contains converted waves as well as shallow layer crustal multiple reflections within the time window of interest, and therefore, its interpretation may be ambiguous. An SRF, on the other hand, is free from S wave multiple reflections within the time window of arrival of converted phases from the deeper discontinuities. In recent times, the SRF technique has become an effective tool to map uppermost mantle discontinuities such as the LAB (e.g., Li et al., 2004; Kumar et al., 2005a, 2005b, 2006, 2007; Kawakatsu et al., 2009; Kumar and Kawakatsu, 2011; Rychert et al., 2005; Sodoudi et al., 2006; Zhao et al., 2010; Uma Devi et al., 2011; Kayal et al., 2011; Zhao et al., 2011; Kumar et al., 2011, 2013, 2014). For our analysis, we used waveforms from earthquakes of magnitudes >5.5mb, within teleseismic distance ranges (P waves: 30°–90°; S waves: 60°–85°; and SKS waves: 85°–120°) from all available back azimuths. PRF and SRF are practically identical in analysis except that the role of each component is interchanged. To isolate the weak Sp (or Ps as the case may be) phase from S (or P), we further rotate the Z-R-T components into P-SV-SH components using an incidence angle derived from the minimum SV energy on the P component at zero time in order to have an optimal isolation of P-SV-SH (e.g. Kumar et al., 2005a,b, 2006; Kumar and Kawakatsu, 2011). In the presence of large noise and strong lateral heterogeneity, incidence angles determined in this way may be erroneous, and therefore, the events with incidence angles >52° are discarded. This coordinate rotation ensures a clean decomposition of P-to-s (S-to-p). Once the traces are rotated into P and SV components, we employ source normalization using deconvolution. Here we adopted a time domain deconvolution technique (Berkhout, 1977). In case of P-RF, the SV is deconvolved with P while for S-RF, P is deconvolved with SV. The distance effect due to different source distributions in receiver functions is corrected for by applying a moveout correction using a

reference slowness of 6.4 s/deg (Yuan et al., 1997) with the global IASP91 Earth model (Kennett and Engahl, 1991).

RECEIVER FUNCTIONS IMAGING BELOW THE CAMBAY RIFT

In the present study, data from 15 broadband seismic stations (Fig. 1) deployed in the western part of the Indian plate was analysed. Images were constructed using good quality 726, S-to-p receiver functions. The image of the Lithosphere-Asthenosphere Boundary (LAB) thus generated is shown in Fig. 2 along two profiles. Figure 2 reveals that there are at least two prominent phases corresponding to conversions from the Moho (Crust-Mantle boundary) and the LAB (marked in the figure) representing a velocity increase across Moho and decrease across LAB. The lithosphere is found to be the thinnest (~60 km) beneath the Cambay rift and deepens to ~110 km on the western side of the profile (towards the coast). Because of the lack of appropriate data, structure beneath the eastern side cannot be ascertained. The lithosphere further shallows towards the coastal region, as observed in profiles AB and CD, probably due to the combination of rift and/or sampling the edge of the oceanic lithosphere. The average lithospheric thickness below the Indian shield is ~100 km (Kumar et al., 2007; Kumar et al., 2013).

The representative stack traces along the profile AB (shown in Fig. 1) at four places along the seismic section are modeled with simple flat layer synthetics. Waveform modeling shows that the lithosphere is ~60 km thick below the rift and on the flank it deepens to ~110 km (Fig. 3). We found that the shear velocity drop across the LAB to be ~10%. The possible reason for this drop in velocity is given below.

DISCUSSION

Nature of Lithosphere-Asthenosphere Boundary below Rift

We noted that the seismic observations were made at short periods (0.25 Hz), the transition (sharpenss) in LAB beneath the Cambay rift is likely to be less than ~15 km with a Vs drop of ~10%. Such a rapid decrease in Vs cannot be reconciled with temperature alone, and an additional mechanism is needed. Inclusion of little more than 1% melt in the asthenosphere in addition to the temperature contrast provides a realistic explanation of this velocity drop (Hammond and Humphreys, 2000) (Fig. 3). The core-refracted shear wave (SKS-waves) studies reveal anisotropy with a delay of 1.6 sec (Mandal, 2011), while the local shear wave (S-waves) splitting results suggest that the crustal anisotropy is of the order of 0.1sec (Mandal, 2009). The large shear wave velocity contrast of 10% (for vertically
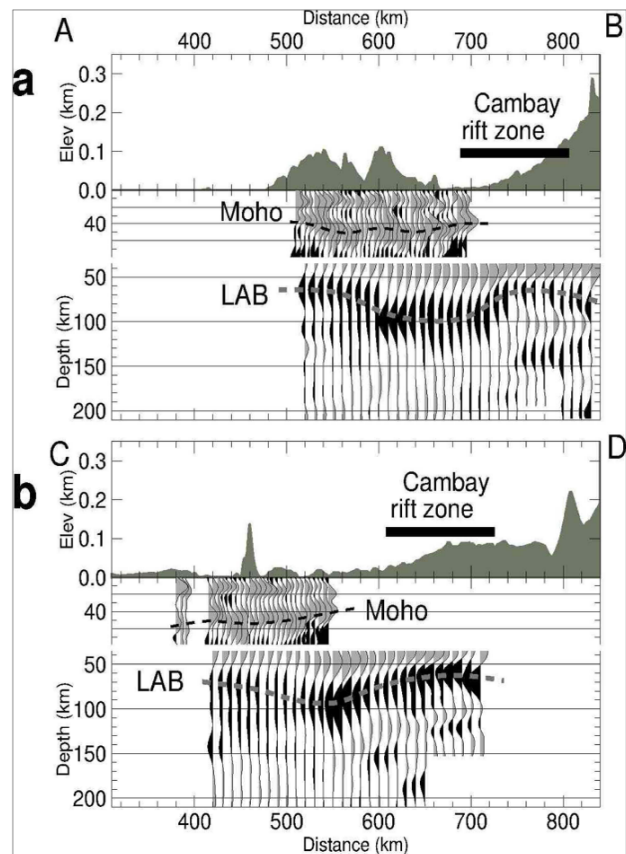

Fig.2. The receiver function data along the two profiles shown in Fig.1. The traces have been generated after moveout correction at a reference slowness of 6.4 s/deg using a global IASP91 earth model. The traces are smoothed with a narrow bin of width of 20 km. In both the plots (a) and (b), the positive polarity phases within the time window of 0-50 km arise from the crust-mantle discontinuity (i.e. Moho) and are plotted at a depth of 40km. Other negative polarity phases identified deeper than 50 km are interpreted as conversions from the LAB and are plotted at a S-to-p conversion depth of 100 km. The profiles are made after projecting the data on either side with ±1 deg. At the top panel of each subplot show the elevation. The thick horizontal line indicates the approximate location of the Cambay rift zone.

propagating SV waves) at the LAB, as observed in the dataset, cannot be attributed to anisotropy. One likely explanation is that the partial melt is distributed as laminar lenses in the asthenosphere (Fig. 3), as has been described in the case of the Pacific plate (Kawakatsu et al., 2009). Such a distribution can explain the large reduction in vertically propagating SV- wave velocity and observed anisotropy. Earlier interpretation of the results of P-to-s conversion and surface wave dispersion indicates similar amount of melt in the asthenosphere in this region (Mandal, 2012).
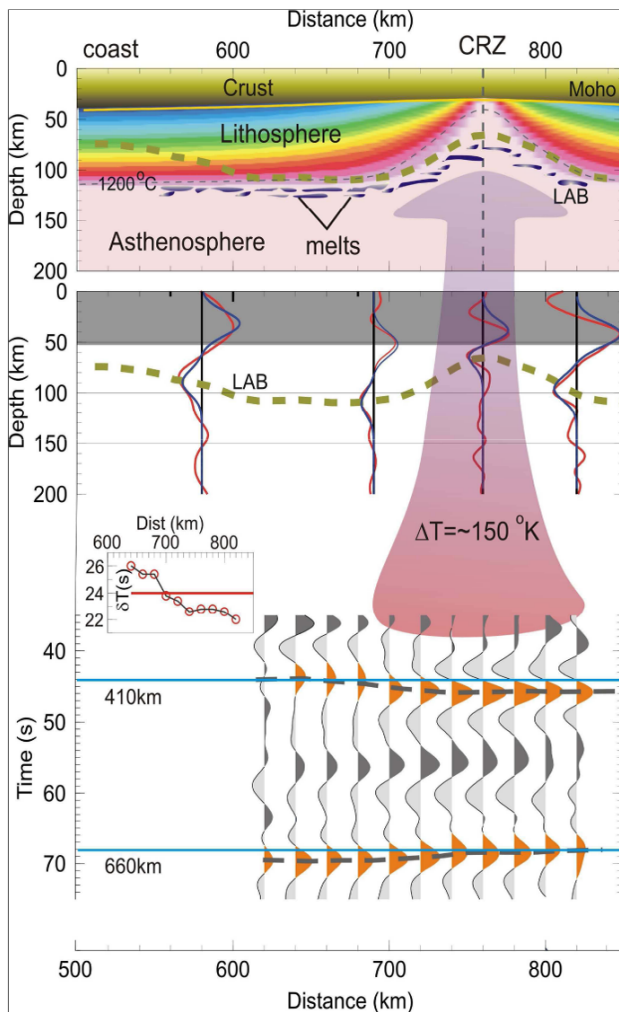
Fig.3. Geodynamic model and waveform modeling. In the top panel the colour represents the isotherm with gray dash like is 1200° C isotherm. Blue broken horizontal blobs are the melt associated with the LAB, where we observed sharp and large Vs drop by ~10%. The representative stack traces at four places across the Cambay rift (Fig. 1), bottom panel, where red are the stack traces with the narrow geographical area and blue are the synthetics data. The thick green line is the LAB surface where it is shallower below Cambay rift (marked as plume track) and deeper beyond that. The gray region in the bottom panel is the approximate crustal part of the waveforms which do not present the true geographical location. So in this plot we should concentrate only on the lithospheric structure. The lower panel shows P-to-s receiver functions showing the upper mantle global discontinuities plotted at 520 km depth. The wiggles are plotted at every 20 km bin with an overlapping bin of 50 km. The 410- and 660- km discontinuities clearly show that they are delayed with respect to the global average and the maximum delay is westward. The transition zone thickness is also shown as inset which clearly reveals that effect of upper mantle heat anomaly as shown by a cartoon.

The converted waves from upper mantle discontinuities (410 km and 660 km) were also analysed. These discontinuities mark the upper and lower boundaries of the mantle transition zone, and mineralogically interpreted as phase transitions from α-olivine to β-spinel, and from γ-spinel to perovskite+magnesiowüstite, respectively. The Clapeyron slopes of the equilibrium phase boundaries indicate that the depth of the '410' discontinuity should be deflected upwards in regions of colder temperature, whereas the '660' should be deflected downwards. The topography of the '410' and '660' discontinuities can therefore provide information about thermal structure in the mantle transition zone. In the Cambay region, the global upper mantle 410-discontinuity shows delay with respect to the global average underneath the rift, while 660-km shows delay shifted westward.; furthermore, the upper mantle transition zone is thinner by ~2sec below the Cambay rift zone (Fig. 3). This delay in transition zone implies that the mantle is at least ~150 °K hotter than the ambient mantle, and the source of heat is located in the upper mantle.

Geotherm below Cambay Rift

Heat flow measurements in the northern part of Cambay Basin show a high range: 75-96 mW/m² with a mean value of 83±7 mW/m² (e.g. Gupta et al. 1970). Other studies inlcuding the bottom hole temperature measurements (Panda and Dutta, 1985; Sonal et al. 2013) show higher geothermal gradient ranging from 20 to 75 beneath Cambay basin. Making the reasonable assumption that heat transfer in the upper 60 km beneath Cambay rift occurs conductively, a set of geotherms (dT/dP gradient) may be extrapolated to 60 km, which are shown as dashed curves in Fig. 4 (dashed curves c, b, a). Although the dT/dP may be steep (i.e., 30°C/km) down to a depth of ~15 km, it should flatten out gradually with depth, i.e., the rate of temperature increase with depth must progressively slow down to 60 km. For comparison purpose, a field of pressure-temperature estimates for mantle xenoliths that occur in nearby Kutch area has been included (e.g., Sen et al., 2009). Because the xenoliths came from a 66 million year old lithosphere at Kutch, the xenolith-based P,T values may not be exactly comparable with the present geotherm at Cambay. The comparative studies of the geothermal curves in Fig.4 suggest that cooling over this period would have lowered the temperature by about 150-200°C at 50-60 km. Therefore, dT/dP gradient (b) may be more representative of the current Cambay rift.

In order to investigate whether or not partial melting may be taking place at the present time beneath Cambay rift, we compare mantle peridotite solidus with and without
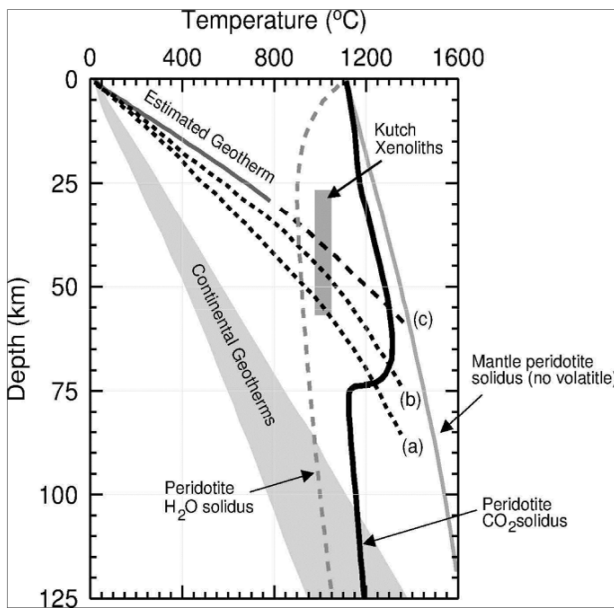
Fig.4. Geotherm in the Cambay Rift. The black line is the estimated geotherm (c) for northern section of the Cambay Basin for the gradient estimated of 30 °C/km. Other two sets of estimated geotherms are also plotted with different gradients (see text for detail discussion) of 20 °C/km (curve a) and 25 °C/km (curve b). The volatile-free peridotite solidus is based on Hirschmann (2000); Peridotite-CO_2 solidus is based on Gudfinnsson & Presnall (2005); and Peridotite-H_2O is estimated on the basis of Wyllie (1978). The gray box area indicates the Kutch xenolith based P-T estimates constructed on the basis of Sen et al. (2009). The dark gray shaded region indicated as continental geotherms are also shown for comparison. Extrapolated Cambay geotherm (dashed line) intersects the peridotite-CO_2 solidus at about 60 km, which is the depth where basaltic melt would be expected to form from a carbonated peridotite beneath Cambay rift. The presence of basaltic melt at such depth is consistent with the occurrence of a sharp LAB in this area.

volatiles are (CO_2, H_2O) in Fig. 4, which shows that our extrapolated geotherms (a) and (b) meet the carbonated perdotite solidus at about 65-70 km, and volatile-free solidus at much greater depths. If the 10% velocity decrease at the LAB beneath Cambay rift is a result of partial melting, then,

based on Fig. 4, it is unlikely that volatile-free melting of mantle peridotite could produce such melts. On the other hand, there is little doubt that CO_2-bearing peridotite could potentially melt at ~65 – 75 km depth. As noted by many previous workers, the "ledge" on the solidus of CO_2 would force such rising volatile-rich low % melts to freeze and fracture the base of the lithosphere, thereby producing a sharp LAB. As an aside, note that the LAB beneath Cambay Basin cannot be due to melting of a hydrated upper mantle because in such a case partial melts would be produced at a much shallower depth (~40-50 km) as indicated by the intersection of geotherms (a) and (b) with the peridotite-H_2O solidus.

CONCLUSIONS

Several lines of evidence suggest the presence of magma beneath Cambay rift basin: sharp drop in seismic shear wave velocity at a depth of ~60km, high heat flow beneath the Cambay rift basin, interaction between mantle solidus and geothermal gradient, and relatively high temperatures recorded by mantle xenoliths from the nearby area of Kutch.

Interestingly, the 410-km discontinuity beneath Cambay rift appears to be consistently delayed by ~2 sec, while 660-km discontinuity appears to have normal velocity. This implies an excess temperature of ~150 °K for Clapeyron slope of 2.9 MPaK^{-1} for the 410 km discontinuitiy (Bina and Helffrich, 1994). We suggest that this excess temperature is due to a thermal plume presently rising from the top of the transition zone and is responsible for triggering melting beneath Cambay.

In summary, our study suggests that the "inactive" Cambay rift zone may not be inactive after all. A thermal plume rising from the transition zone may be trigering magma formation and aiding the thinning of the lithosphere.

References

Basu, A.R., Renne, P.R., Dasgupta, D.K., Teichmann, F. and Poreda, R.J. (1993) Early and late alkali igneous pulses and a high-3He plume origin for the Deccan flood basalts. Science, v.261, pp.902–906.

Berkhout, A. J. (1977) Least square inverse filtering and wavelet decomposition. Geophysics, v.42, pp.1369–1383.

Bina, C.R. and Helffrich, G. (1994) Phase transition Clapeyron slopes and transition zone seismic discontinuity topography. Jour. Geophys. Res., v.99, pp.15853–15860.

Biswas, S.K. (1987) Regional tectonic framework, structure and

evolution of the western marginal basins of India, Tectonophysics, v.135, pp.305-327.

Biswas, S.K. (1999) A Review on the Evolution of rift basins in India during Gondwana with especial reference to Western Indian basins and their Hyderocarbon prospects, Proc. Ind. Nat. Sci. Acad., v.65(3), pp.261-283.

Farra, V. and Vinnik, L. (2000) Upper mantle stratification by P & S receiver functions. Geophys. Jour. Int., v.141, pp.699–712.

Gudfinnsson, G.H. and Presnall, D.C. (2005) Continuous gradations among primary carbonatitic, kimberlitic, melilititic,

basaltic, picritic, and komatiiticmelts in equilibrium with garnet lherzolite at 3-8 Gpa. Jour. Petrology, v.46, pp.1645–1659.

GUPTA, M.L., VERMA, R.K., HAMZA, V.M., RAO, G.V. and RAO, R.U.M. (1970) Terrestrial heat flow and tetonics of the Cambay basin, Gujart, India, Tectonophysics, v.10, pp147-163.

HAMMOND, W.C. and HUMPHREYS, E. D. (2000) Upper mantle seismic wave velocity: Effects of realistic partial melt geometries. J.our Geophys. Res., v.105, pp.10975--10986.

HIRSCHMANN, M.M. (2000) Mantle solidus: experimental constraints and the effects of peridotite composition. Geochem. Geophys. Geosyst. doi: 2000GC000070.

KAWAKATSU, H., KUMAR, P., TAKEI, Y., SHINOHARA, M., KANAZAWA, T., ARAKI, E. and SUYEHIRO, K. (2009) Seismic Evidence for sharp Lithosphere-Asthenosphere Boundaries of Oceanic Plates. Sci., v.324, pp.499-502, doi: 10.1126/science. 1169499.

KAYAL, J.R., SRIVASTAVA, V.K., KUMAR, P., CHATTERJEE, R. and KHAN, P. K. (2011), Evaluation of crustal and upper mantle structures using receiver function analysis: ISM broadband observatory data. Jour. Geol. Soc. India, v.78, pp.76–80, doi:10.1007/ s12594-011-0069-5.

KENNETT, B.L.N. and ENGDAHL, E.R. (1991) Traveltimes for global earthquake location and phase identification, Geophys. Jour. Internat., v.105, pp.429-465.

KUMAR, P. and KAWAKATSU, H. (2011) Imaging the seismic litho-sphere-asthenosphere boundary of the oceanic plate, Geochem. Geophys. Geosyst., v.12, doi:10.1029/2010GC0 03358.

KUMAR, P., KAWAKATSU, H., SHINOHARA, M., KANAZAWA, T., ARAKI, E. and KIYOSHI, S. (2011) P and S receiver function analysis of seafloor borehole broadband seismic data, J. Geophys. Res., v. 116, B12308, doi:10.1029/2011JB008506.

KUMAR, P., KIND, R., HANKA, W., WYLEGALLA, K., REIGBER, CH., YUAN, X., WOELBERN, I., SCHWINTZER, P., FLEMING, K., DAHL-JENSEN, T., LARSEN, T. B., SCHWEITZER, J., PRIESTLEY, K., GUDMUNDSSON, O. and WOLF, D. (2005a) Lithosphere-Asthenosphere Boundary in the North-West Atlantic Region, Earth Planet Sci. Lett., v.236, pp.249-257.

KUMAR, P., KUMAR, M.R., SRIJAYANTHI, G., ARORA, K., SRINAGESH, D., CHADHA, R.K. and SEN, M.K. (2013) Imaging the Lithosphere-Asthenosphere Boundary of the Indian Plate using converted wave techniques. Jour. Geophys. Res., v.118, pp.1-13, doi:10.1002/jgrb.50366.

KUMAR, P., TALUKDAR, K. and SEN, M.K. (2014) Lithospheric Structure Below Transantarctic Mountain using Receiver Function Analysis of Tamseis data. Jour. Geol. Soc. India, v.83, pp.483-492.

KUMAR, P., YUAN, X., KIND, R. and KOSAREV, G. (2005b) The lithosphere– asthenosphere boundary in the Tien Shan–Karakoram region from S receiver functions: evidence for continental subduction, Geophys. Jour. Lett., v.32, doi:10.1029/2004GL 022291.

KUMAR, P., YUAN, X., KIND, R. and NI, J. (2006) Imaging the collision of the Indian and Asian Continental Lithospheres Beneath Tibet. Jour. Geophys. Res., v.111, doi:10.1029/ 2005JB003930.

KUMAR, P., YUAN, X., KUMAR, M. R., KIND, R., LI, X. and CHADHA, R.K. (2007) The rapid drift of the Indian tectonic plate, Nature, v.449, pp.894-897, doi:10.1038/nature06214.

LANGSTON, C.A. (1995) Corvallis, Oregon, crustal and upper mantle structure from teleseismic P and S waves. Bull. Seismol. Soc. Amer., v.67, pp.713–724.

LI, X., KIND, R., YUAN, X., WÖLBERN, I. and HANKA, W. (2004)

Rejuvenation of the lithosphere by the Hawaiian plume, Nature, v.427, pp.827–829.

MAHONEY, J. J., DUNCAN, R.A., KHAN, W., GNOS, E. and McCORMICK, G.R. (2002) Cretaceous volcanic rocks of the South Tethyan suture zone, Pakistan: implications for the Réunion hotspot and Deccan Traps, Earth Planet. Sci. Lett., v.203, pp.295-310.

MANDAL, P. (2009) Crustal Shear wave splitting in the Epicentral Zone of the 2001 Mw 7.7 Bhuj Earthquake, Gujarat, India. Jour. Geody., v.47, pp.246-258.

MANDAL, P. (2011) Upper mantle seismic anisotropy in the intra-continental Kachchh rift zone, Gujarat, India, Tectonophysics, v.509, pp.81-92.

MANDAL, P. (2012) Passive source seismic imaging of the crust and upper mantle beneath the 2001 Mw7.7 Bhuj earthquake region, Gujarat. Bull. Seism. Soc. Amer., v.102(1), pp.252-266.

MOHAN, M. (1995) Cambay Basin – A promise of oil and gas potential. Jour. Paleont. Soc. India, v.40, pp.41-47.

PANDA, P.K. and DUTTA, H.C. (1985) Prospective Geothermal Fields in Cambay Basin, India Internat. Symp. Geothermal Energy, pp. 537-538.

RYCHERT, C.A., FISCHER, K.M. and RONDENAY, S. (2005) A sharp lithosphere-asthenosphere boundary imaged beneath eastern North America, Nature, v.436, pp.542–545, doi:10.1038/ nature03904.

SEN, G., BIZIMIS, M., DAS, R., PAUL, D.K. and BISWAS, S. (2009) Deccan plume, lithosphere rifting, and volcanism in Kutch, India. Earth Planet Sci. Lett., v.277, pp.101–111.

SODOUDI, F., YUAN, X., LIU, Q., KIND, R. and CHEN, J. (2006) Lithospheric thickness beneath the Dabie Shan, central eastern China from S receiver functions, Geophys. Jour. Internat., v.166, pp.1363–1367.

SONAM, DHANNAWA, B.S. and VARUN KUMAr (2013) Trend of Geothermal gradient from Bottom Hole Temperature studies in South Cambay Basin (Narmada Broach Block). 10th Biennial Internat.Conf. & Exposition, SPG, P386, Kochi.

STAMMLER, K. (1993) Seismic Handler: programmable multichan-nel data handler for interactive and automatic processing of seismological analysis. Comput. Geosci., v.19, pp.135-140.

UMA DEVI, E., KUMAR, P. and KUMAR, M.R. (2011) Imaging the Indian lithosphere beneath Eastern Himalayan region, Geophys. Jour. Internat., v.187, pp.631–641, doi:10.1111/ j.1365-246X.2011.05185.x.

VINNIK, L.P. (1977) Detection of waves converted from P to SV in the mantle. Phys. Earth Planet. Inter., v.15, pp.39–45.

WESSEL, P. and SMITH, W.H.F. (1995) New version of the Generic Mapping Tools released, Eos Trans. AGU, v.76, pp.33, doi:10.1029/95EO00198.

WYLLIE, P.J. (1978) Mantle fluid compositions buffered in peridotite–CO_2–H_2O by carbonates, amphibole, and phlogopite. Jour. Geol., v.86, pp.687–713.

YUAN, X., NI, J., KIND, R., MECHIE, J. and SANDVOL, E. (1997) Lithospheric and upper mantle structure of southern Tibet from a seismological passive source experiment. Jour. Geophys. Res. v.102, pp.27491–27500.

ZHAO, D., LEI, J., INOUE, T., YAMADA, A. and GAO, S.S. (2006) Deep structure and origin of the Baikal rift zone. Earth Planet. Sci. Lett., v.243, pp.681-691.

ZHAO, W., KUMAR, P., MECHIE, J., KIND, R., MEISSNER, R., WU, Z., SHI, D., SU, H., XUE, G., KARPLUS, M. and TILMANN, F. (2011) Tibetan plate overriding the Asian plate in central and northern Tibet. Nature Geosci., v.4, pp.870-873, doi:10.1038/ngeo 1309.